Florida Center for Advanced Aero-Propulsion (FCAAP) – ***Annual Technical Symposium 2009***

Macro and Microscale DBD Actuators for Improved Flow Management

Chin-Cheng Wang and Subrata Roy

Florida Center for Advanced Aero-Propulsion (FCAAP)
Computational Plasma Dynamics Laboratory and Test Facility
Applied Physics Research Group, University of Florida, Gaineville, FL 32611
{james614, roy}@ufl.edu

Abstract. We present significant developments in the study of dielectric barrier discharge (DBD) plasma actuators for macro and microscale applications. In macroscale, horseshoe shaped actuators are introduced to control the bulk flow penetrating the boundary layer by plasma induced jet turbulizing the flow. Based on the powering scheme of electrodes, these actuators not only induce flow attachment to the work surface but also can extract momentum from an upstream flow injecting it into the bulk fluid. Another application for such actuator predicts film cooling enhancement on gas turbine blades by 100% over the standard baseline design. Traditional macroscale DBD actuators suffer from relatively small actuation effect. As a remedy we propose microscale plasma actuators that may induce orders of magnitude higher force density. We present a concept of plasma micropump using small actuators. Such micro pump delivers a flow rate of tens of ml/min. Such flow rate may be beneficial for many applications from aerospace to biomedical industry.

Keywords: Plasma actuators, electrohydrodynamics, 3-D flow management, micropump, film cooling

1 Introduction

In recent days, surface barrier discharge has been successfully used to control low speed boundary layer flows [1,2]. Such a discharge imparts body force inside the boundary layer of a fluid in the vicinity of an exposed electrode. Examples include mitigation of low speed flow separation on airfoils at a high angle-of-attack, and lift increment and/or drag reduction of airfoils and fuselages. Both pulsed dc and ac powered plasma actuators can induce active control of the neighboring flow dynamics in an instantaneous manner. However, such a control has limited application due to insufficient control of the boundary layer. For example, it will be highly beneficial if we can find an actuator that can penetrate the edge of essentially two-dimensional boundary layer directly modifying the bulk flow through actively diverting the direction of injected momentum. Such modification may allow active tripping of the flow and thus help plasma based heat transfer [3]. Wang and Roy [4] use this idea to actively enhance interaction of cool air jets with hot crossflow for improved cooling of hot surfaces. Also it will be very useful if we may use the same actuator for both mitigating the flow separation and inducing flow turbulization as needed [5].

To understand the physics of plasma actuators, a set of multiscale multispecies basic investigations of plasma actuation was conducted by Roy and his group [6-9]. They demonstrated the model predictions for charge densities, electric field and gas velocity distributions and showed induced wall jets that mimic trends reported in the experimental literature [1,2]. Based on the first-principles analysis using 8 species of air N, N_2, O, O_2, O^- N_2^+, O_2^+, and electrons, Singh and Roy [10] identified a functional relationship between the electric force and electric and geometric control parameters. The magnitude of the approximated force increases with the fourth power of the amplitude of the rf potential. Thus the induced fluid velocity also increases.

The primary weakness of traditional DBD actuators is the relatively small flow actuation effect. It has been proven to be quite effective only at low speeds (10-30 m/s). In order to remedy this weakness, microscale discharge is proposed to increase the higher electrohydrodynamic (EHD) force density with lower power consumption. Although micro-scale discharge has been studied experimentally [11,12] for more than a decade, our understanding of the fundamental physics is still limited due to the challenges in reduced length scales, unsteady phenomena, and rapid collisional interaction in micro gaps. Therefore, numerical simulation is a remedy to overcome the experimental challenges.

The main purpose of this paper is to summarize the following two major developments: (1) Numerical demonstration of a novel horseshoe plasma actuator in bulk flow control by effective turbulization and its influence

in heat transfer management over a turbine blade. We use horseshoe plasma actuator at the downstream (or upstream) of the cooling hole with geometric modification. The intension of the shaped holes is to trip the emerging cold jet and reduce the lift-off effect of the cold jet. (2) For purely flow control application, standard actuators are ineffective at higher speeds due to an inherent low momentum injection limitation by the plasma actuators. As a possible remedy, we study the microscale actuator [13] and apply it to a novel micropumping system [14] using EHD force. The rest of the paper is organized as follows. Section 2 gives the computational details. The results are described in Section 3, and conclusions are drawn in Section 4.

2 Computational Details

A hydrodynamic plasma model is utilized to calculate charge densities (q), electric field (E), and potential distribution (ϕ) at atmospheric pressure. The model uses an efficient finite element algorithm anchored in the multiscale ionized gas (MIG) flow code [6,13]. The unsteady transport for electrons and ions is derived from conservation laws in the form of mass conservation equation. The species momentum is modeled using the drift-diffusion approximation under isothermal condition. Such assumption is justified for atmospheric pressure. The charge species of positive ion n_i and electron n_e, i.e. $\beta = i, e$, are derived from first principles in the form of conservation of species continuity $\partial n_\beta / \partial t + \partial n_\beta V_{\beta j} / \partial x_j = \alpha |\Gamma_e| - r n_i n_e$, where $\alpha = Ap \exp[-B/(|E|/p)]$ is Townsend coefficient, and the working gas is nitrogen at bulk pressure p = 760 torr and room temperature T = 300 K. The electron flux is given as $|\Gamma_e| = \sqrt{(n_e V_e)_x^2 + (n_e V_e)_y^2}$, and the electron-ion recombination rate r is derived from Kossyi *et al*. [15]. The drift-diffusion approximated charge momentum results in $n_\beta V_{\beta j} = \mathrm{sgn}(e) \partial n_\beta \mu_\beta E_j - D_\beta \partial n_\beta \partial x_j$, where μ_β species mobility and D_β species diffusion coefficient [16] for the ion at 300 K as well as electron at 11600 K, and the electric field $E_j = -\partial\phi / \partial x_j$ is the negative gradient of electric potential. The relation between electric potential and charge separation is given by the Poisson equation $\partial / \partial x_j \left(\varepsilon \partial\phi / \partial x_j \right) + e(n_i - n_e) = 0$, where ε is the dielectric constant, and e is the elementary charge. Above equations are normalized with reference time $t_0 = 10^{-9}$ sec and reference density $n_0 = 10^{17}$ m^{-3}. Due to several orders of magnitude difference in timescales of plasma and gas flow, we employ the time average of electric body force $F_j = e(n_i - n_e)E_j$ in the Navier-Stokes equations $\rho \mathrm{D}V_j / \mathrm{D}t = \rho F_j - \nabla_j p + \mu \nabla^2 V_j$, where μ is the viscosity of fluid.

2.1 Horseshoe actuators

The geometry in Fig. 1(a) shows the powered electrode consists of a half circle with two extended ends in the shape of a horseshoe. The grounded electrode is on the other side of dielectric with the same shape but smaller. There is a 2 mm gap between two electrodes. The origin ($x = y = 0$) is at center of the half circle, and the ends of half circle extend from y = 0 to y = -7 mm. We have studied four cases H1 to H4 in this article with different flow directions and polarities. One may modify horseshoe actuator and connect it one by one, and then become a serpentine actuator configuration as described in Roy and Wang [5]. We use the time averaged body force based on first principle simulation of Singh and Roy [10]. The potential is applied to the exposed electrode with $\phi = \phi_0 \sin(2\pi ft)$ V. For such horseshoe device several kN/m^3 force density may be obtained by spending a few watts.

2.2 Plasma actuated film cooling

Fig. 2(a) describes schematic control volume of freestream air passing over a flat surface (e.g., a turbine blade). This surface of study has a row of injection holes through which the cool air is issued at an angle $\alpha = 35°$. The cool jet at temperature T_j = 150K is injected into the hot freestream of T_{fs} = 300K. The injection ducts are circular pipes with diameter equal to d = 2.54mm. The actuator is located at the downstream of the cooling hole, where the powered and grounded electrodes are kept at a sequence to push the fluid in the forward direction. The selected mean flow velocities, static pressures and temperatures (i.e., densities) in the injection pipe and the wind tunnel gives a blowing ratio M = 1. The inlet section is located at x = -20d and the exit is located at x = 29d. The other dimensions and boundary conditions are shown in [4]. Fig. 2(b) inlay shows schematics of various shapes of the hole exit plane: A

for baseline, B for bumper with 0.5*d* height, C for jet hole with compound slopes, and D for rectangular slot. We impose the time averaged force density based on a phenomenological force density parameter Λ_f described in [4]. Note that for standard actuation device a local $\Lambda_f \sim 10$ kN/m^3 may be obtained with a few input watts per meter length of the actuator. For film cooling problem with high upstream velocity an imposed $\Lambda_f \sim 2000$ kN/m^3 requires kW/m level power for the actuator.

2.3 Microscale actuators for EHD micropump

We simulate plasma-gas interactions inside a plasma micropump shown in Fig 3(a). The micro plasma pump consists of four pairs of DBD actuators at both inlets and two pairs of DBD actuators at the center of the pump. The pump inlet openings are 250 μm at both sides and the single outlet opening is 500 μm at the top. Fig. 3(b) shows the configuration of DBD actuator. The powered electrode is 20 μm wide, while the grounded electrode is 40 μm wide. The gap between electrodes is 10 μm at streamwise direction and 50 μm in vertical direction. We simulate the symmetric half of the micro pump with 67x50 elements and 13635 nodes. The walls of the micropump are made of Kapton polyimide insulator with dielectric constant $\varepsilon_d = 4.5\varepsilon_0$, where ε_0 is permittivity of vacuum. The boundary condition of potential ϕ is equal to 1300 V. We neglect the thickness of powered electrode (at $y = 0.5$ and 3) and grounded electrode (at $y = 0$ and 3.5). For the flow simulation, gauge pressure is equal to zero at the inlet and the outlet. The right boundary is maintained as symmetry, and based on low Kn [17] all dielectric surfaces are maintained at zero wall velocity.

3 Results and Discussion

3.1 Horseshoe actuators

Five cases were simulated for this problem: One base case without plasma actuation, four cases related to horseshoe actuators. These actuators provide a three dimensional plasma actuation in both streamwise and crosswise directions, and the boundary layer is significantly influenced in low speed regime by induced velocity. Fig. 1(b) shows a significant tripping resulting in local increase in boundary layer thickness (δ) almost 10 times from 0.002 to 0.02 m, and a sharp increase and decrease in pressure coefficient (C_p) at the plasma region along the streamwise direction. This is because the fluid changes its direction and tries to move upward. Fig. 1(c) shows that the streamwise velocity V_y for case H1 to H4 on the *yz*-plane ($x = 0$) show clockwise vortex induced by plasma actuation in case H1 and H3, and a counterclockwise vortex generated in case H2 and H4. For case H1 and H4, we find the highest streamwise velocity very close to the wall. For case H2, a strong plasma actuation which is close to the wall pushes the fluid in streamwise and crosswise directions away from the centerline of the actuator, so there is a stagnation region along the centerline. For case H3, the inward plasma force accumulates the fluid toward the centerline of the actuator, and pinches it upward.

3.2 Plasma actuated film cooling

Fig. 2(b) shows the effect of geometric modifications of the cooling hole with and without plasma. The computed centerline effectiveness η for the baseline case without plasma discharge compares reasonably with the experimental data and other previously reported numerical results. The performance plots of different hole shapes show that C and D have a better η before $x/d = 6$ because the expansion of the jet reduces the momentum ratio, increasing the cooling performance. Also, the step at the edge of D acts as a trip for the cold fluid inducing more attachment. Interestingly, case B provides a higher η beyond $x/d = 20$ because the jump effect delays the cold fluid attached to the work surface. With plasma of $\Lambda_f = 2000$ kN/m^3, the η increases by over 70%, 558%, 137%, and 164% more, respectively, at $x/d = 5$ for designs A-D. It is evident that the plasma flow control guarantees the flow attachment on the surface, improving the heat transfer drastically. Fig. 2c plots the temperature distribution on the same planar location ($x/d =$ 4, 10, and 16) and marks *y*-*z* plane temperature distribution at $x/d = 4$ with plasma for arrangement D. The cold jet bends (trips) and under the influence of plasma induced electric force becomes significantly attached to the work surface. More details of these results have been reported by Wang and Roy [4].

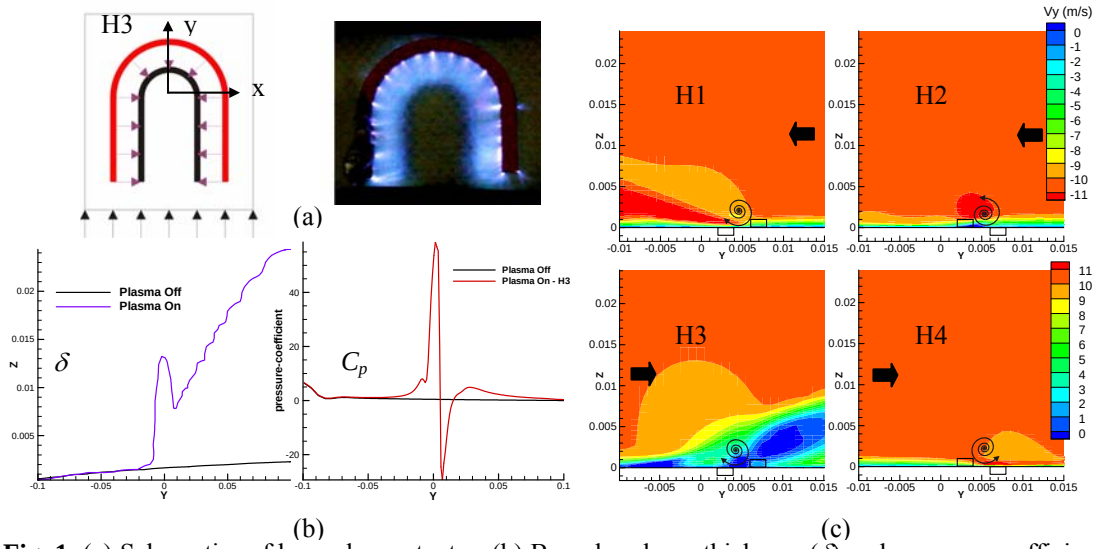

Fig. 1. (a) Schematics of horseshoe actuator. (b) Boundary layer thickness (δ) and pressure coefficient (C_p) along streamwise direction. (c) Streamwise velocity V_y for various flow configurations at $x = 0$.

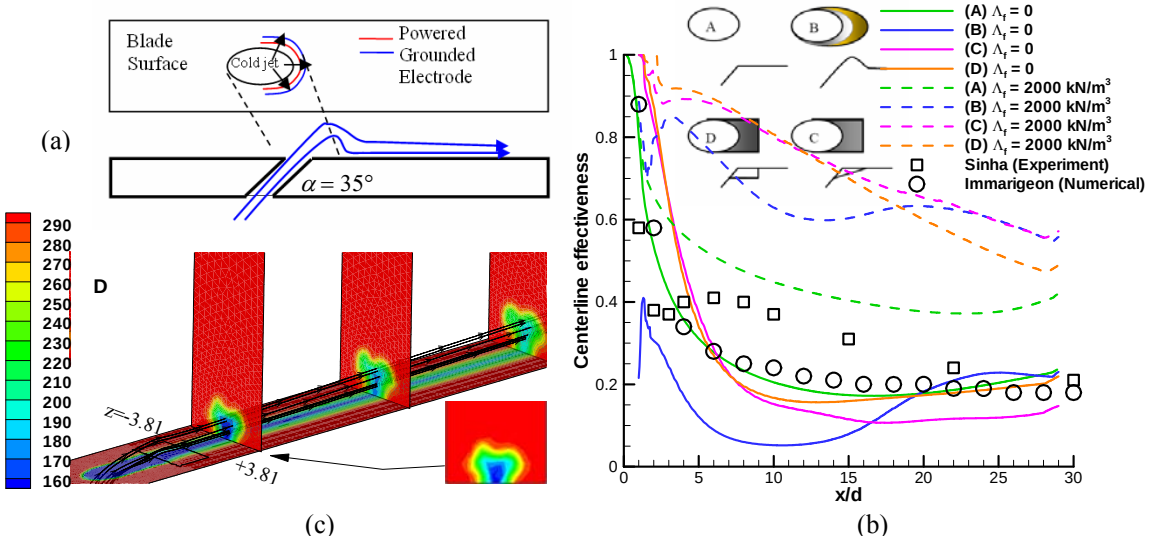

Fig. 2. Schematics of plasma actuated heat transfer for (a) adiabatic flat plate with plasma actuator, (b) Centerline effectiveness with inlay of different cooling hole types A through D, and (c) Temperature distribution on select planes show best cooling performance using plasma in design D.

3.3 Microscale actuators for EHD micropump

Microscale actuators have not been explored for flow control application. Fig. 3(c) shows that the computed electric field compared with the published experimental data of Longwitz [18] with a very good agreement from 50 to 5 μm inter-electrode gaps. The computed charge density slightly decreased as the gap g decreased, but it increased at the gap below 10 μm because much less electrons exist in the plasma region. Based on the calculation of the electric force (qE), we can see the force F_y is 1 MN/m^3 at 20 micron gap. Note that such force density is three orders of

magnitude higher than that of macro plasma actuators. As the gap decreases force seem to increase sharply. For example, at five micron gap the force density increases approximately seven fold to 6.8 MN/m^3.

Fig. 4(a) shows an applied potential of 1300 volts on the powered electrode (red). The electric field lines are acting from the powered electrode to the grounded electrode. Due to a large difference of potential between electrodes, the fluid is ionized at local regions shown in Fig. 4(b). We can see the net charge densities are concentrated inside the boundary layer near the powered electrode, and it is almost zero away from the wall. Fig. 4(c) shows the flow behavior inside the micro plasma pump. We can see the plasma drives the fluid into the pump at the inlet due to the net near-wall jet created by DBD actuators. The actuator close to right boundary is used for altering the fluid flow direction from horizontal to vertical direction and pushes the fluid upward to the outlet. However, it also creates a strong vortical structure inside the pump. The V_y-velocity increases sharply from the wall (at x = 0.0005 m) and becomes flat V_{max} = 3.1 m/s at middle of the pump (at x = 0.00075 m). The sharp increase is because the shear stress that flow exerts on the wall of the pump. After simple calculation, we find the maximum flow rate Q_{max}= 46.5 ml/min.

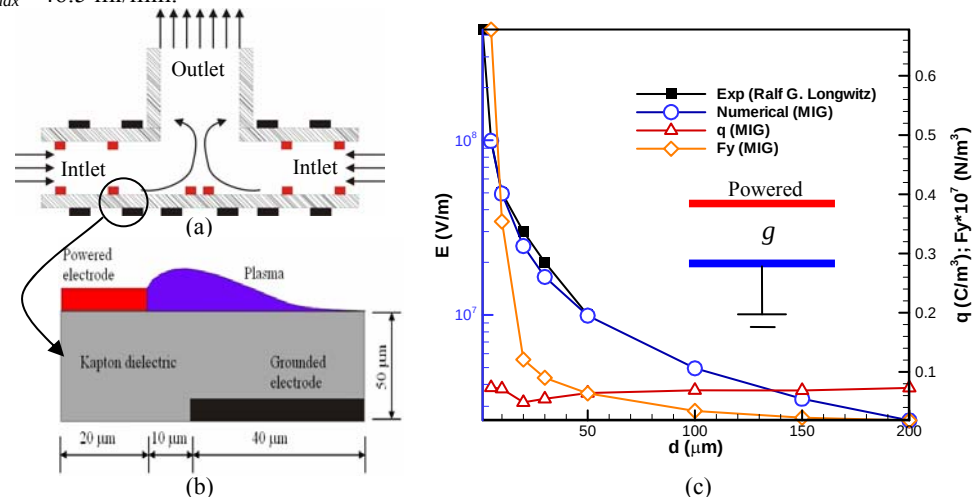

Fig. 3. (a) Schematic of micro plasma pump. (b) Schematic of microscale DBD actuator. (c) Experimental validation of numerical prediction at microscales for g = 5 to 50 μm..

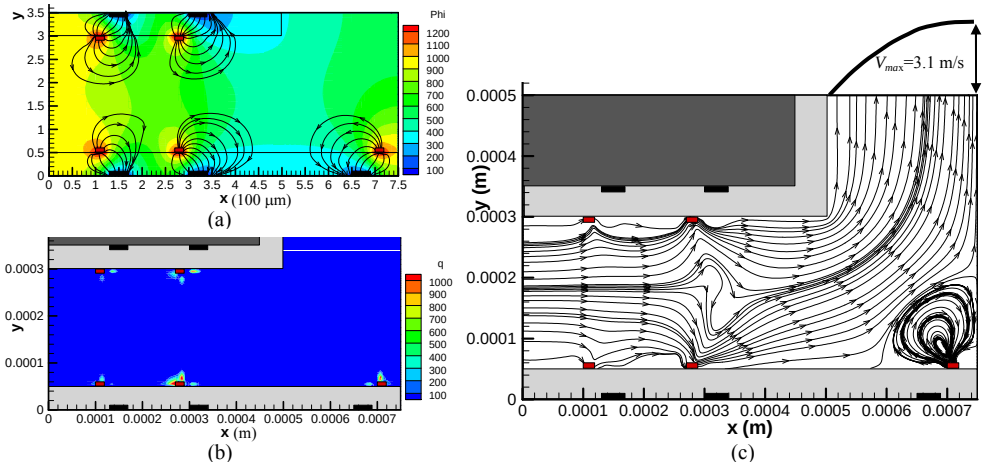

Fig. 4. (a) Potential distribution (ϕ) with electric potential lines. (b) Charge density contour (q) with reference density 10^{17} m^{-3}. (c) The velocity stream traces inside the micropump.

4 Conclusions and Future Work

We have studied realistic applications of DBD actuators in both macro and microscale using two-species hydrodynamic plasma model coupled with Possion equation using finite element based multiscale ionized gas (MIG) flow code. The *new horseshoe plasma actuator* was simulated to predict full three-dimensional control. Documented results for several electrical and geometric arrangements show active modification of the boundary layer thickness suitable for tripping and flow attachment using the same actuator. We apply such actuators for improving the film cooling. The results show an increase in cooling effectiveness by at least 100%. The geometric modifications using various hole shapes with plasma actuation shows a significant improvement of effectiveness than standard design. Plasma augmented design modified flow control ideas may become more beneficial for cases with badly separated jets at higher velocity ratio. Simulation of *new microscale plasma actuators* predicts three orders of magnitude (MN/m^3) higher thrust density than their macroscale counterparts. For *a patented microscale plasma pump*, we predict a flow rate of 46.5 ml/min. Such flow rate may be useful for the application of biological sterilization and decontamination, micro propulsions, and cooling of microelectronic devices. Inside micro plasma pump a vortical structure may affect the volumetric flow rate. This may be avoided by adjusting the location of actuators and the input voltage. Realistic PIV testing is underway to validate these designs.

5 Acknowledgments

This work was partially supported by the Florida Center for Advanced Aero-Propulsion (FCAAP). The authors also acknowledge partial support of AFOSR and AFRL grants for this research.

References

[1] Roth, J.R., Sherman, D.M., Wilkinson, S.P., "Boundary Layer Flow Control with an One Atmosphere Uniform Glow Discharge Surface Plasma," 36th AIAA Aerospace Sciences Meeting and Exhibit, AIAA 1998-0328.
[2] Benard, N., Balcon, N., Moreau, E., "Electric Wind Produced by a Surface Dielectric Barrier Discharge Operating in Air at Different Pressures: Aeronautical Control Insights," Journal of Physics D: Applied Physics, vol. 41, no. 4, (2008) 042002.
[3] Roy, S., Wang, C.C., "Plasma actuated heat transfer," Applied Physics Letters, 92 (2008) 231501.
[4] Wang, C.C., Roy, S., "Electrodynamic Enhancement of Film Cooling of Turbine Blades," J. Appl. Phys., 104, (2008) 073305.
[5] Roy, S., Wang, C.C., "Bulk Fluid Modification with Horseshoe and Serpentine Plasma Actuator," Journal of Physics D: Applied Physics, vol. 42, (2009) 032004.
[6] Roy, S., "Flow actuation using radio frequency in partially-ionized collisional plasmas," Appl. Phys. Lett., 86 (2005) 101502.
[7] Roy, S., Gaintonde, D., "Force Interaction of High Pressure Glow Discharge with Fluid Flow for Active Separation Control," Physics of Plasmas, vol. 13, no. 2, (2006) 023503.
[8] Singh, K.P., S. Roy and D. Gaitonde, "Study of control parameters for separation mitigation using asymmetric single dielectric barrier plasma actuator," Plasma Sources Science & Tech, 15 (2006) 735-743.
[9] Singh, K.P. and S. Roy, 2007, "Modeling plasma actuators with air chemistry for effective flow control," J. Appl. Phys., 101 (2007) 123308.
[10] Singh, K.P., Roy, S., "Force Approximation for a Plasma Actuator Operating in Atmospheric Air," J. Appl Phys. 103, (2008) 013305.
[11] Ono, T., Sim, D.Y., Esashi, M., "Micro-discharge and Electric Breakdown in a Micro-gap," J. Micromechanics and Microengrg., 10, (2000) 445-451.
[12] Torres, J.M., Dhariwal, R.S., "Electric Field Breakdown at Micrometre Separations," Nanotechnology, vol. 10, (1999) 102.
[13] Wang, C.C., Roy, S., "Microscale Plasma Actuators for Improved Thrust Density," J. Appl. Phys., 106 (2009) in press.
[14] Roy, S., "Method and apparatus for efficient micropumping," International Patent Publication number PCT WO 2009/015371 dated Jan 29, 2009.
[15] Kossyi, I.A., Kostinsky, A.Y., Matveyev, A.A., Silakov, V.P., "Kinetic Scheme of the Non-equilibrium Discharge in Nitrogen-oxygen Mixtures," Plasma Sources Science and Technology, vol. 1, (1992) 207-220.
[16] Surzhikov, S.T., Shang, J.S., "Two-component Plasma Model for Two-dimensional Glow Discharge in Magnetic Field," Journal of Computational Physics, vol. 199, (2004) 437-464.
[17] Roy, S., Raju, R., Chuang, H.F., Cruden, B.A., Meyyappan, M., "Modeling Gas Flow Through Microchannels and Nanopores," Journal of Applied Physics, vol. 93, no. 8, (2003) 4870-4879.
[18] Longwitz, R.G., "Study of Gas Ionization in a Glow Discharge and Development of a Micro Gas Ionizer for Gas Detection and Analysis," PhD thesis, Institute of Microsystems and Microelectronics, Swiss Federal Institute of Technology, Lausanne, Switzerland (2004).